Probing Atlas model atmospheres at high spectral resolution. Stellar synthesis and reference template validation

4 authors, including:

Some of the authors of this publication are also working on these related projects:

Project   The Globular cluster system of M31. View project

Project   Solar Radio Emission in the National Laboratory of Space Weather View project

**Astronomy
&
Astrophysics**

Probing Atlas model atmospheres at high spectral resolution

Stellar synthesis and reference template validation

E. Bertone[1], A. Buzzoni[2], M. Chávez[1], and L. H. Rodríguez-Merino[1]

[1] INAOE - Instituto Nacional de Astrofísica, Óptica y Electrónica, Luis Enrique Erro 1, 72840 Tonantzintla, Puebla, Mexico
e-mail: [ebertone;mchavez;lino]@inaoep.mx
[2] INAF - Osservatorio Astronomico di Bologna, Via Ranzani 1, 40127 Bologna, Italy
e-mail: buzzoni@bo.astro.it

ABSTRACT

Aims. The fast improvement of spectroscopic observations makes mandatory a strong effort on the theoretical side to better reproduce the spectral energy distribution (SED) of stars at high spectral resolution. In this regard, relying on the Kurucz ATLAS/SYNTHE original codes we computed the BLUERED library, consisting of 832 synthetic SED of stars, that cover a large parameter space at very high spectral resolution ($R = 500\,000$) along the $3500-7000$ Å wavelength range.
Methods. BLUERED synthetic spectra have been used to assess in finer detail the intrinsic reliability and the performance limits of the ATLAS theoretical framework. The continuum-normalized spectra of the Sun, Arcturus, and Vega, plus a selected list of 45 bright stars with high-quality SEDs from the Prugniel & Soubiran ELODIE catalog, form our sample designed to probe the global properties of synthetic spectra across the entire range of H-R parameters.
Results. ATLAS models display a better fitting performance with increasing stellar temperature. High-resolution spectra of Vega, the Sun, and Arcturus have been reproduced at $R = 100\,000$, respectively, within a 0.7%, 4.5%, and 8.8% relative scatter in residual flux. In all the three cases, the residual flux distribution shows a significant asymmetry (skewness parameter $\gamma = -2.21, -0.98, -0.67$, respectively), which neatly confirms an overall "excess" of theoretical line blanketing. For the Sun, this apparent discrepancy is alleviated, but not recovered, by a systematic decrease (-40%) of the line oscillator strengths, $\log(gf)$, especially referring to iron transitions. Definitely, a straight "astrophysical" determination of $\log(gf)$ for each individual atomic transition has to be devised to overcome the problem. By neglecting overblanketing effects in theoretical models when fitting high-resolution continuum-normalized spectra of real stars, we lead to a systematically warmer effective temperature (between +80 and +300 K for the solar fit) and a slightly poorer metal content.

Key words. Sun: atmosphere – stars: atmospheres – stars: individual: Arcturus – stars: individual: Vega – stars: fundamental parameters – line: profiles

1. Introduction

Spectral synthesis of stars, across their different location in the H-R diagram, is a strategic tool for a number of important astrophysical applications, dealing both with the study of the fundamental parameters of individual objects (e.g. Soubiran et al. 1998; Bertone et al. 2004a; Valenti & Fischer 2005), and/or with overall distinctive properties of stellar aggregates, through population synthesis procedures (e.g., Worthey 1994; Vazdekis et al. 1996; Yi et al. 1998; Bruzual & Charlot 2003; Buzzoni 2005).

An accurate and self-consistent match of model atmospheres, including up-to-date physical ingredients and appropriate treatment of the energy transfer mechanisms, is critical to confidently calibrating the empirical templates, linking effective temperature and surface gravity with observable quantities like spectral type and luminosity class (see, e.g., Böhm-Vitense 1981, for a review). In this regard, a theoretical approach is usefully complemented by direct empirical calibrations, mainly relying on measurements of the apparent stellar radii (r) and emitted luminosity (L) to estimate the effective temperature (T_{eff}) of stars, via the fundamental equation $L = 4\pi r^2 \sigma T_{eff}^4$ (e.g., Johnson 1966; Ridgway et al. 1980; di Benedetto & Rabbia 1987; di Benedetto 1998; Alonso et al. 1999; Wittkowski et al. 2004).

In any case, despite dramatic improvements in the operational algorithms and input physics, modeling of stellar atmospheres still proves to be a formidable task, only marginally eased by the stronger computing power available nowadays. In the recent years, the theoretical effort had to face the impressive wealth of high-quality observational data as a result of a combined contribution of new-generation telescopes and high-resolution spectrographs, which boosted the study of bright nearby stars and distant galaxies at unprecedented spectral resolution and accuracy levels.

In this framework, detailed and exhaustive libraries of theoretical stellar fluxes are required to fully exploit the large amount of information provided by the observations. Among the most recognized and popular codes for model atmosphere computation and spectral synthesis (for wide coverage in spectral type and luminosity, see Gustaffson et al. 1975; Hauschildt et al. 1999; Shulyak et al. 2004; for more restricted types, see Tsuji 1976; Werner 1986; Hubeny & Lanz 1995; Santolaya-Rey et al. 1997; Hillier & Miller 1998; Pauldrach et al. 2001; Behara & Jeffery 2006), the Kurucz (1970, 1979) ATLAS code certainly stands as a milestone for its wide range of application along nearly three decades of research in stellar astrophysics.

Following a continual upgrade process, the original version of the code has now grown further, and the most recent

releases of ATLAS (Kurucz 1992a, 1995) include several million spectral lines accounting for nearly all the most important di-atomic molecules. Still, the lack of H_2O and other tri-atomic molecules, and an incomplete treatment of TiO opacity prevents, however, a suitable match of stars cooler than 3500 K (Kurucz 1992a; Castelli et al. 1997; Bertone et al. 2004a), although important preliminary efforts to implement water vapor and the Ly-α H−H and H−H$^+$ quasi-molecular absorptions Castelli & Kurucz 2001), certainly represent a noticeable advance for the modeling of M stars.

Based on ATLAS model atmospheres, in the recent years a number of new collections of synthetic spectra upgraded the Kurucz (1979) original calculations, exploring the (T_{eff}, log g, [M/H]) parameter space at different steps and spectral resolving powers. Among others, this includes the work of Chavez et al. (1997), who computed a high-resolution grid ($R = \lambda/\Delta\lambda = 250\,000$) of 711 stellar spectra along the wavelength range $\lambda\lambda$ 4850−5400 Å, covering most of the popular absorption features used in the Lick narrow-band spectrophotometric system (Faber et al. 1985; Worthey et al. 1994). More recently, Munari & Castelli (2000) and Castelli & Munari (2001) computed a grid of synthetic spectra at $R = 20\,000$ in the T_{eff} range from 3500 to 50 000 K, originally conceived to test the spectroscopic performances of the Global Astrometric Interferometer for Astrophysics satellite (GAIA; Katz et al. 2004). This library has then been expanded in wavelength ($\lambda\lambda$ 2500−10 500 Å; Munari et al. 2005) and degraded to $R = 11\,500$ and 2000 such as to match spectroscopic data of the Radial Velocity Experiment (RAVE; Steinmetz 2003) and of the Sloan Digital Sky Survey (SDSS; Gunn & Knapp 1993).

Again, Martins et al. (2005) extended the wavelength coverage ($\lambda\lambda$ 3000−7000 Å) of the Gonzalez-Delgado & Leitherer (1999) original set of synthetic spectral energy distributions (SEDs) to explore local thermodynamical equilibrium (LTE) versus non-LTE effects in model atmospheres across the range $50\,000 \geq T_{eff} \geq 3000$ K. These models make use of the PHOENIX spherical LTE model atmospheres (Hauschildt et al. 1999b) for stars cooler than 4500 K, while ATLAS LTE atmospheres cover the T_{eff} range up to 25 000 K, and TLUSTY non-LTE models (Hubeny & Lanz 1992) match hotter temperatures.

Furthermore, the Barbuy et al. (2003) synthetic stellar spectra, based on modified ATLAS model atmospheres, have been further elaborated by Coelho et al. (2005) to produce near-infrared SED ($\lambda \rightarrow 1.8\,\mu$m) of F to M stars, relying on the FANTOM synthesis code by Spite (1967) and Cayrel et al. (1991). These models include revised chemical opacities and tuned oscillator strengths, as well as α-enhanced metallicity composition.

In addition, it is also worth mentioning the systematic coverage of the ATLAS parameter domain carried out by Murphy & Meiksin (2004), consisting of 6410 stellar SEDs between $50\,000 \geq T_{eff} \geq 5250$ K at $R = 250\,000$ along the 3000−10 000 Å wavelength interval); while, to analyse the stellar populations of star clusters in the Magellanic Clouds, Leonardi & Rose (2003) complemented an empirical stellar library with a grid of synthetic spectra computed with the Kurucz SYNTHE code at $R = 72\,700$ in the 3500−5500 Å interval.

In this regard, the blue/ultraviolet spectral range ($\lambda\lambda$ 850−4700 Å) has been further probed at high resolution ($R = 50\,000$) by the UVBLUE library of Rodriguez-Merino et al. (2005). This consists of 1770 synthetic spectra spanning a wide combination of fundamental parameters, with $50\,000 \geq T_{eff} \geq 3000$ K, $0 \leq$ log $g \leq +5.0$ dex

and $-2.0 \leq [M/H] \leq +0.5$. Given the extremely wide ramifications of the Kurucz work and the variety of derived spectral grids available to date, it is of paramount importance, we believe, to assess in finer detail the intrinsic reliability of the ATLAS theoretical framework and to evaluate on a quantitative basis its performance limits as an interpretative tool for the investigation of single stars and stellar aggregates.

In this paper, we want, therefore, to further carry on such a "validation" process, following the previous important input of Bessell et al. (1998) and Castelli et al. (1997). Our analysis will rely on the new BLUERED grid of synthetic spectra (preliminarily presented in Bertone 2001; Bertone et al. 2003a, 2004b, and discussed, in more specific detail in Sect. 2). This library comprises a bulk of 832 theoretical SEDs exploiting the extremely high spectral resolution allowed by the SYNTHE code ($R > 500\,000$). For their coverage and resolution, these new models intend to provide a best-suited operational test-bed to probe ATLAS performances at the highest possible spectral detail[1]. In Sect. 3, we will focus our analysis on three very special stellar templates, namely the Sun, Arcturus, and Vega, which represent a benchmark for the different physical regimes of stars across the H-R diagram. In that section we also proceed to test the properties of the synthetic SEDs by comparison with a selected sample of 45 K- to F-type stars from the ELODIE high-resolution catalog by Prugniel & Soubiran (2001). The results of our comparisons, and the implied feedback for theoretical model atmospheres will be summarized in Sect. 4.

2. Bluered: an $R = 500\,000$ library of stellar SEDs

Our calculations are based on ATLAS9 code (Kurucz 1993a, 1995), under the so-called "classical-model approximation". This assumes a plane-parallel geometry for LTE atmospheric layers in hydrostatic equilibrium, and with fixed chemical composition. The physical variables are constant with time, and global (i.e., radiative and convective) energy flux is conserved. In this upgraded version, atmospheric spatial resolution has been increased to 72 mesh points, and calculations encompass a range in the Rosseland optical depth from log $\tau_{Ross} \sim 2$ "outward" to log $\tau_{Ross} \sim -7$. The radiation field is probed in 1221 wavelength points, from 90 Å to 160 μm.

Line blanketing is computed statistically by means of opacity distribution functions (ODF), which average the contribution of the different atomic/molecular species through the corresponding oscillator forces (Strom & Kurucz 1966; Kurucz 1970, 1979). The prevailing contribution of iron (and iron-peak) elements is accounted for by means of an updated list of nearly 42 million lines (Kurucz 1992a, 1993b) out of a total of about 60 million lines of atoms and diatomic molecules. Atomic species are traced up to nine ionization stages (Kurucz 1995).

Convection treatment relies on the standard mixing length theory by Böhm-Vitense (1958); the mixing length parameter is set to $\ell/H_p = 1.25$ and the microturbulence velocity $\xi = 2$ km s^{-1} throughout. For our model atmospheres we also chose to implement the so-called "approximate overshooting" mechanism, according to Castelli et al. (1997), which ostensibly provides a better match of Sun's SED (Castelli et al. 1997, see the next section for a more detailed analysis of this possibly important point).

The parameter space covered by BLUERED model atmospheres is summarized in Fig. 1 and Table 1. The plot

---

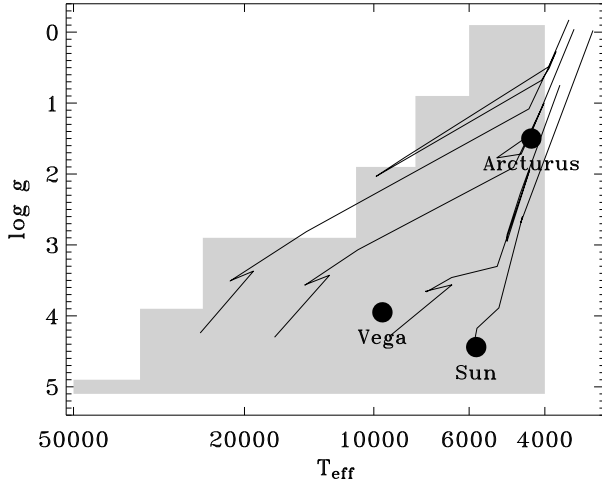[1] BLUERED is available, upon request, in the World Wide Web site http://www.inaoep.mx/~modelos/bluered/bluered.html

Table 1. Main properties of the BLUERED synthetic stellar library.

Wavelength range	$3500 \rightarrow 7000$ Å
$R = \lambda/\Delta\lambda$	500 000
$\Delta\lambda$ sampling step	$0.007 \rightarrow 0.014$ Å
No. of wavelength points	346 645
$T_{\rm eff}$	$4000 \rightarrow 10\,000$ K @ step of 500 K
	$10\,000 \rightarrow 35\,000$ K @ step of 1000 K
	$35\,000 \rightarrow 50\,000$ K @ step of 2500 K
log g	$0.0 \rightarrow 5.0$ dex @ step of 0.5 dex
[M/H]	$-3.0, -2.0, -1.0, -0.3, 0.0, +0.3$ dex
No. of absorption lines	more than 46 millions
Molecular species	C_2, CN, CO, CH, NH, OH, MgH, SiH, SiO, TiO
No. of spectra	832

displays the theoretical grid for solar metallicity (a similar coverage is also assured for the other [M/H] values), compared in the log g vs. log $T_{\rm eff}$ plane with four illustrative stellar tracks for 1, 2, 5, and 10 $M_\odot$, from Girardi et al. (2000) and Salasnich et al. (2000) and with the location of the three relevant templates (namely Vega, Arcturus, and the Sun), which we will discuss in the following section. Effective temperature is explored over the full spectral-type range from K to O stars ($T_{\rm eff}$ = 4000 → 50 000 K), while surface gravity accounts for the $I - V$ MK luminosity classes. Six metallicity values are accounted for in the library, including the case of extremely metal-poor Pop II stars ([M/H] = −3) up to super metal-rich stars of [M/H] = +0.3. Each metallicity subset consists of 138−140 spectra, for a total of 832 model atmospheres and their corresponding high-resolution SED. Metal abundances are solar-scaled, assuming the Anders & Grevesse (1989) chemical abundances for the Sun.

2.1. The spectral grid overall properties

Adopting as input the ATLAS9 model atmospheres computed by Kurucz[2], we carried out spectral synthesis calculations by means of the Kurucz (1993a,b) SYNTHE code. At this stage, the theoretical code overcomes the forced simplifications of ATLAS9 ODFs and explicitly accounts for individual atomic/molecular transitions to assess monochromatic chemical opacity at each wavelength point. This is certainly an advantage as far as we try to reproduce spectral features at very high resolving power, as one can easily tune up any single elemental abundance within the model.

One has to be aware, however, that this process is, in fact, strictly self-consistent only for those fixed chemical mixtures matching the ATLAS ODFs. By allowing somewhat prominent deviations from this reference chemical abundances, a subtle physical mismatch might arise in the ATLAS/SYNTHE interface leading to a nominal "unphysical" output for the resulting SED.

The BLUERED synthetic SEDs span the wavelength interval 3500−7000 Å computed at a resolving power R = 500 000.

[2] http://kurucz.harvard.edu/grids.html

Accordingly, the sampled wavelength step $\Delta\lambda = \lambda/R$ ranges from 0.007 to 0.014 Å, in the UV and red extremes, respectively (see Table 1)[3]. The overall interval includes all the Balmer series and the complete set of features measured by the Lick/IDS spectrophotometric indices (Worthey et al. 1994; Trager et al. 1998), as well as by other relevant narrow-band spectrophotometric systems, such as that of Rose (1994) and of Vazdekis & Arimoto (1999). As for the photometric broadband systems, the Johnson B and V, the Thuan-Gunn g, the Sloan g', and the Washington M passbands are entirely comprised within the computed wavelength interval.

A full contribution of diatomic molecules in the relevant spectral range has been considered in SYNTHE (especially for G-K stars), including optical/NIR transitions for C_2, CN, CO, CH, NH, OH, MgH, SiH, and SiO. As an effort to produce more reliable spectra at the low-temperature edge of the grid (including K-M stars), we also made use of the large TiO line list (37 million entries) as updated by Schwenke (1998) and implemented in SYNTHE by Kurucz (1999). This list replaces the older one (Kurucz 1992a) still included, however, in the ATLAS ODFs. Although within the limits of its partial implementation in the codes, this improvement is of special importance for our output, as TiO results to be the prevailing opacity source in stars cooler than 4000 K (see Milone & Barbuy 1994, for a discussion)[4]. Air wavelengths have been adopted for line calculations and no rotational broadening is applied to the spectra.

2.2. Caveats

The assumptions and approximations of the "classical model atmospheres", as well as the (in)completeness of the input data, forcefully affect our spectra, so one must keep in mind their shortcomings. A discussion of these issues is present in Rodriguez-Merino et al. (2005), who made use of the same Kurucz's model atmospheres. However, we want to stress a few important points.

---

[3] BLUERED output consists of two quantities, namely the normalized emerging flux density per unit wavelength, i.e., $F'(\lambda) = F(\lambda)/(\sigma T_{\rm eff}^4)$, and the residual flux, i.e. $(F/F_c)(\lambda)$, which is the ratio of the emerging flux over the theoretical continuum emission. Note that the flux normalization makes straightforward the library implementation for stellar population synthesis models (see, e.g. Bertone et al. 2003b, 2005; Buzzoni et al. 2005).

[4] However, given the vanishing contribution of molecules with increasing temperature, to speed up computations we only included TiO for spectra cooler than $T_{\rm eff}$ = 5000 K, while no molecules at all are considered for stars warmer than $T_{\rm eff}$ = 8000 K.

The plane-parallel geometry is less suitable to describing giant and supergiant stars, where atmospheric layers can extend over a large fraction of the total radius. Microturbulence velocity, besides changing with optical depth also tends to increase with increasing effective temperature, therefore a constant value of 2 km s^{-1}, adopted by BLUERED, underestimates the line broadening in early-type stars. We expect that this effect can produce higher T_{eff} and $\log g$ values by flux-fitting with BLUERED spectra such a class of objects, since the missing microturbulence contribution must be compensated for by higher Doppler and pressure broadenings. Neither rotation nor wind velocity fields are considered; therefore, much care should be paid when dealing with fast rotators or hot stars where the hydrostatic equilibrium does not hold.

So-called "predicted lines" (those for which the energy of one or both levels of the transition are theoretically derived) can be affected by a large error in wavelength (up to several angstroms), which makes them unsuitable for high-resolution analyses (e.g., Kurucz 1992b; Munari et al. 2005). We, therefore, did not include these lines in the input for SYNTHE, while they are taken into account in the opacity calculation of the input model atmospheres. This choice may affect the overall flux distribution, especially in the UV, where the contribution of a large number of "predicted" absorption lines from the iron group elements are omitted in BLUERED. Finally, we note that the presence of chromosphere, magnetic fields, and surface inhomogeneities are not considered in our models.

3. Model validation at the different temperature ranges

Any effective validation of model atmosphere theory should naturally rely on the detailed comparison of synthetic spectra with the observed SED of well-observed reference stars, ideally probing the different regions across the H-R diagram. This type of analysis requires first-rank observations taken at the highest spectral resolution and superior signal-to-noise ratio (S/N), such as to provide a useful "feedback tool" to refine theoretical input-physics and achieve a better modeling of real stars. Two important issues can, in principle, be effectively tackled in our discussion, dealing with *a)* a fine-tuning process of atomic oscillator forces ($\log(gf)$); and *b)* the role of molecules in cool-star synthesis.

As for the first point, a comparison with the Sun data is of course an unavoidable step in our analysis, while Arcturus stands out as a suitable target to assess the latter topic. In addition, a detailed comparison with the data of Vega will allow us to expand our discussion to the high-temperature regime. It is worth stressing that we do not intend to investigate the detailed impact of non-LTE treatment of atomic species. Short & Hauschildt (2003, 2005) have computed non-LTE model atmospheres and SEDs for the Sun and Arcturus pointing out that, in addition to a similar trend for LTE models, non-LTE calculations produce an even higher flux in the blue and near-UV regions. They mainly ascribe this effect to the overionization of Fe I (e.g., Rutten 1988; Shchukina & Trujillo Bueno 2001) and conclude that further opacity sources in the UV are evidently still missing in the modeling of stellar atmospheres. We would encourage more focused investigations of this important issue as they may provide crucial feedbacks to improve both the physics of model atmospheres and line parameters.

3.1. The Sun at R = 522 000 and the gf tuning

The Sun is obviously the more immediate and important template to be considered in our analysis; it is the only star for which we have complete and detailed information on its surface brightness distribution and for which we can measure its emerging flux at extremely high spectral resolution and signal-to-noise ratio.

From the observational side, various spectral atlases at different wavelength ranges and accuracy levels have been collected in the last decades starting with the pioneering contribution of Minnaert et al. (1940), who provided the first detailed solar spectrum at optical range. Then, it is worth reporting the work of Mohler (1950), McAllister (1960), Delbouille et al. (1973), Hall (1973), Milone et al. (1974), Cohen (1981), Brekke (1993), and Samain (1995), while Wallace et al. (1996), first extended the observations to the near and mid infrared range. Finally, Thuillier et al. (1997), first explored the ultraviolet range by means of rocket- and space-borne observing missions.

One of the most complete data collections, and currently a reference source for the study of the solar spectrum at optical and near-infrared wavelength, is certainly the "Solar Flux Atlas from 296 to 1300 nm" of Kurucz et al. (1984), providing the solar irradiance spectrum (also in a version where the flux has been normalized at the local pseudo-continuum) at an unprecedented resolution of $R = 522\,000$ and $S/N \geq 3000$. These data have been tackled relying on the ATLAS Sun model (SUNK94: $T_{\text{eff}} = 5777$ K, $\log g = 4.4377$, as discussed by Castelli et al. 1997), for which we derived the synthetic SED from 3500 to 7000 Å at a resolving power $R = 2\,000\,000$. Again, reference chemical abundances in our model are those of Anders & Grevesse (1989), with the same published line list. To match the observation, the synthetic spectrum was then broadened "ad hoc", using a Gaussian kernel to consider the effects due to macroturbulence ($v_{\text{macro}} = 1.5$ km s^{-1}, Gurtovenko & Kostik 1981) and a two-term elliptic plus parabolic profile (e.g., Royer 2005) to account for rotation ($v_{\text{rot}} = 2.0$ km s^{-1}, e.g. Pierce & Lopresto 1984) of the Sun. Finally, we reduced the spectral resolution to $R = 522\,000$, assuming a Gaussian instrumental profile.

In Fig. 2, we show the residual distribution of the theoretical minus observed SED, both normalized at their corresponding pseudo-continuum[5]. Some spectral regions in the Sun atlas, like the intervals near 6300 and 6900 Å, severely affected by telluric features, have been masked out in the figure and not included in our comparison.

The figure provides useful hints for an accurate diagnostic of the model input physics. We see, in fact, that the plot is made up of a dense sequence of positive and negative spikes, which mainly track the residual flux differences in the absorption line profiles. While positive spikes in the residual distribution mostly originate from observed lines that do not have a synthetic counterpart at the same wavelength, the negative peaks come from theoretical absorption lines that are weaker or undetected in the observed spectrum. Both positive and negative spikes tend to decrease in amplitude with increasing wavelength, indicating a better match of theory and observations, and no systematic drift is present in the data distribution, thus reassuring on the adopted value of T_{eff} in the model.

---

[5] Note that, according to our definition, the *absolute residuals* of normalized fluxes, $r = (f_{\text{syn}}/f_{\text{syn}}^{\text{c}}) - (f_{\text{obs}}/f_{\text{obs}}^{\text{c}})$ (label "c" denoting the "pseudo-continuum"), like in Fig. 2, are equivalent, to a first approximation, to *relative flux residuals* in the sense $r' = (f_{\text{syn}} - f_{\text{obs}})/f_{\text{obs}}$, provided one avoids strong absorption lines. More generally, we could write $r = r' f_{\text{obs}}$, being $f_{\text{obs}} \lesssim 1$ the normalized observed flux.
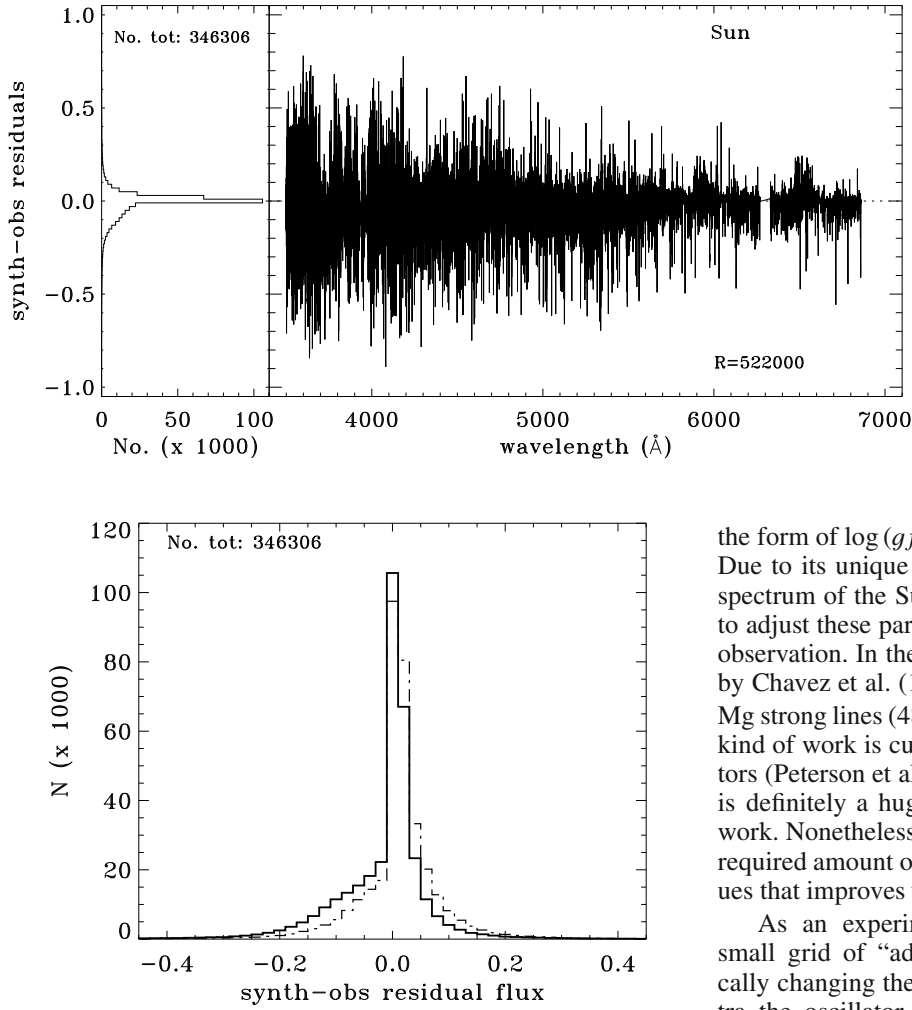
Fig. 3. Histogram of the residuals (synthetic-observed) for the solar spectrum in the wavelength regions 3500−6270 Å and 6330−6860 Å, using the original line list (*solid line*) and the line list where the $\log(gf)$ values of all atomic lines were decreased by 0.2 dex (*dashed-dotted*).

The global (i.e., positive and negative) root-mean-square (rms) value of the residual distribution of the plot of Fig. 2 is $\sigma(r) = 0.089$ (which means, in other words, that observed solar SED is reproduced within roughly a 9% relative flux uncertainty), with a systematic offset between the spectra of $\langle \Delta f_c/f_c \rangle = -0.014$ overall[6]. The distribution of the flux residuals, reported in more expanded detail in the histogram of Fig. 3 (solid line), shows a markedly skewed distribution toward negative values (the skewness value is $\gamma(r) = -0.98$)[7]. *Quite remarkably, this is a striking indication for the synthetic SED to display an excess of stronger (and/or partially unmatched) absorption lines compared to the observations.* Bell et al. (1994) found a similar behavior using a line list extracted from the Kurucz database and a MARCS solar model (Gustafsson et al. 1975) with $T_{eff} = 5800$ K.

The systematic overestimate of line depth is partially due to the line physical parameters adopted in the Kurucz' atomic line list. Among them, the oscillator strength value – usually given in

the form of $\log(gf)$ – is the one that most affects the line depth. Due to its unique qualities of spectral resolution and S/N, the spectrum of the Sun could be, in principle, used as a reference to adjust these parameters, to reach an optimum match with the observation. In the optical region, this task has been performed by Chavez et al. (1997) in a relatively small interval around the Mg strong lines (4800−5400 Å). In the mid-UV regime the same kind of work is currently performed by Peterson and collaborators (Peterson et al. 2001). However, this trial-and-error process is definitely a huge task and is well beyond the scope of this work. Nonetheless, it could be of special interest to indicate the required amount of change to apply, on average, to $\log(gf)$ values that improves the solar fit.

As an experiment in this regard, we have computed a small grid of "ad hoc" synthetic solar spectra by systematically changing the adopted $\log(gf)$ scale. In a first set of spectra the oscillator strength of all atomic transitions has been decreased accordingly, by a fixed offset such as $\Delta \log(gf) = -0.10, -0.15, -0.20, -0.25, -0.30, -0.35$ and -0.40 dex; conversely, in a second set of models we applied the same $\Delta \log(gf)$ offset to iron lines *only*. Finally, the same procedure was applied in a third set of calculations to *non-iron atomic lines alone*. The derived rms values of the solar fit, like in Fig. 2, are summarized in Fig. 4. All three curves show a clear minimum, with the iron atomic transitions (comprising 9757 lines vs. a total of 23 680 absorption features in the considered wavelength range) playing a major role in constraining the fit accuracy.

Overall, the results of our exercise show that a roughly 40−50% *weaker* oscillator strength (mainly restrained to iron atomic transitions) certainly allows a better fit to the solar observations (see the dashed histogram in Fig. 3). On the other hand, and even more importantly, one has also to admit that such a correction, by itself, *cannot drastically improve the match of the theoretical model*, but just decreases the residual rms with the observed solar SED by less than 1%. Therefore, this leads us to conclude that *(i)* a straight "astrophysical" determination of the oscillator strength for each individual atomic transition should be devised; and *(ii)* a substantial improvement of the physics, which involves the line formation in the ATLAS models, is still required.

To quantify the effect that overblanketing produces on the assessment of the main stellar physical parameters (T_{eff}, $\log g$, $[M/H]$) we have determined the best fiducial parameters for the Sun using the BLUERED grid. We have used the same procedure as in Bertone et al. (2004a), minimizing, in this case, the rms of the relative flux residuals ($f_{syn} - f_{obs}$). We obtained a best

---

[6] This value also places an upper limit at roughly 1.5% the relative uncertainty in settling the pseudo-continuum, according to our comparison procedure.

[7] We computed the skewness as $\gamma(r) = \langle \mu_3 \rangle / \langle \mu_2 \rangle^{3/2}$, where μ_n is the nth central moment.
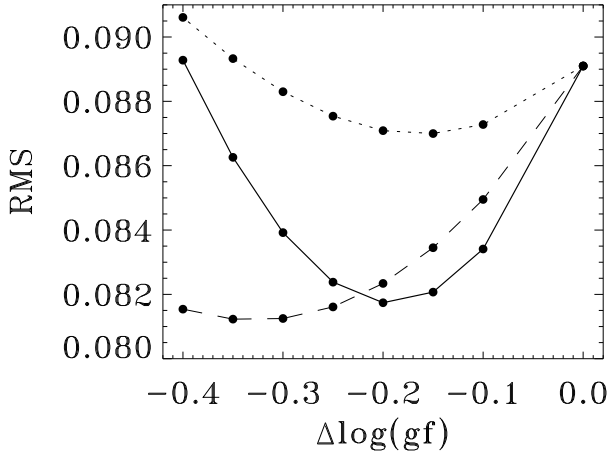
Fig. 4. The rms value of the comparison of the synthetic and observed solar spectrum as a function of the $\log(gf)$ modification for all atomic lines(*solid line*), only Fe lines (*dashed*), and all lines except Fe (*dotted*).

fiducial effective temperature and surface gravity for each metallicity grid. The absolute minimum rms = 0.0848 has been obtained for the combination $(T_{\mathrm{eff}}/\log g/[M/H])$ = $(5860/5.0/-0.3)$, which means about 80 K warmer, 0.50 dex higher surface gravity and half the metallicity with respect to the solar accepted values. However, if we only restrain the comparison to the solar metallicity, we obtain a minimum rms = 0.0863 for $(6130/5.0/0.0)$, which has the same gravity as the previous result, but a T_{eff} 270 K higher. We stress that our results have been obtained using normalized fluxes and not SEDs, whose shape are strongly dependent on the effective temperature. Our results are only based on the relative depths of absorption features.

The warmer estimated temperature for the Sun is due to the fact that, to reach a better agreement with the observation, the residual flux at the core of a majority of the absorption lines should be higher; this can be obtained by increasing the T_{eff}, which lowers the electron population of the levels involved in the majority of the lines. At the same time, to compensate for the decrement in the equivalent width, the surface gravity should also be larger to increase the pressure broadening of the lines. This is consistent with the results found by Buzzoni et al. (2001) who matched a sample of observed spectra with a grid of synthetic ones at mid resolution: a temperature excess implies a gravity excess, too. In fact, for the solar metallicity case and for a $\Delta T_{\mathrm{eff}} = 6130-5777$ K, Eq. (9) in Buzzoni et al. (2001) predicts a $\Delta \log g = 0.40$ dex, which is in agreement with the difference of 0.56 dex between the Sun and our solar-metallicity best fit.

We repeated the procedure of recovering the solar parameters by comparing the irradiance spectrum of the Sun (Kurucz et al. 1984) with BLUERED spectra, whose flux was normalized to the observed at 5550 Å. In this case, besides the line absorption profiles, we took the overall energy distribution into account by the minimization process. We compared the physical quantity $(f_{\mathrm{syn}} - f_{\mathrm{obs}})/f_{\mathrm{syn}}^{\mathrm{c}}$ [8]. The results show that, at solar metallicity, a minimum rms = 0.095 is found for the combination $(5840/5.0/0.0)$, which is a temperature 290 K lower than the one previously obtained by comparing normalized spectra. The addition of the information on the spectral energy shape reduces the error caused by the overblanketing of the input line

---

[8] Note that the flux difference is divided by the theoretical continuum level to give more weight to the wavelength points with higher emerging flux, which means that the emphasis is on reproducing the overall shape of the energy distribution rather than the line center values.

Table 2. Adopted chemical abundance for the Arcturus model.

Element ratio	Element ratio
[N/Fe] = +0.3	[Si/Fe] = +0.4
[O/Fe] = +0.4	[Ar/Fe] = +0.4
[Ne/Fe] = +0.4	[Ca/Fe] = +0.3
[Na/Fe] = +0.3	[Sc/Fe] = +0.2
[Mg/Fe] = +0.4	[Ti/Fe] = +0.3
[Al/Fe] = +0.3	

list. However, both the T_{eff} and $\log g$ of the Sun are still overestimated. Removing the constraint over the metallicity, the best fiducial parameters are $(5710/5.0/-0.3)$ with an rms = 0.088; again, the temperature is 150 K lower than the one obtained from spectra normalized to unity.

However, the quality of the synthetic lines not only depends on the parameters that directly determine their profile, such as the oscillator strength, the damping constants, or the transition energy, but also on the many tunable parameters that are used to compute the model atmosphere and the spectrum, the most important being the assumed solar chemical composition. A change in these latter parameters would imply a redefinition of the former. Considering the very large number of lines present in our SEDs, we did not perform a meticolous time-consuming trial-and-error line fitting of the solar spectrum to tune each individual line parameter. An automatic procedure for performing this task would be very valuable; we are currently working in this direction. Of course, the ideal solution to reduce the discrepancy with the observations is to improve the line list using the best data available from laboratory experiments.

3.2. Arcturus and the molecular contribution in cool stars

Arcturus (α Bootis, HD 124897, HR 5340, K1.5–2 III) is one of the brightest red giant stars in the sky; it is therefore a good target for spectroscopic observations at very high resolution. The low temperature of the photospheric layers allows several diatomic molecules to form. In addition, Ryde et al. (2002) discovered water vapor in the Arcturus infrared spectrum and claimed that it forms in the photosphere. We can use Arcturus to assess the impact of the molecular bands on the high-resolution spectrum modelling. Griffin (1968) and Hinkle et al. (2000) have both produced high-resolution optical spectra of Arcturus. The Griffin atlas covers the interval 3600−8825 Å at a $R \sim 130\,000$. The Hinkle et al. (2000) atlas is complemented by an infrared and an ultraviolet spectra (Wallace & Hinkle 1996; Hinkle et al. 2005) to cover almost all the bolometric emission, from 1150 Å to 5.3 μm.

In this work, we adopted the optical spectrum by Hinkle et al. (2000), which has been observed at a resolving power $R \sim 150\,000$ and signal-to-noise ratio of about 1000. The observation spans the 3727−9300 Å wavelength interval, which includes almost all the BLUERED range. We computed a synthetic spectrum using a 72-layer model atmosphere computed by Kurucz[9] with $T_{\mathrm{eff}} = 4300$ K and $\log g = 1.5$ dex. The overall metallicity is $[M/H] = -0.5$ dex, with some element abundances enhanced by 0.2−0.4 dex (see Table 2 and in particular Luck & Heiter 2005, for the Ti (over)abundance). The microturbulence velocity is variable with depth, from 0.98 km s^{-1}, at the surface, to 3.58 km s^{-1} at the bottom of the atmosphere. The physical

---

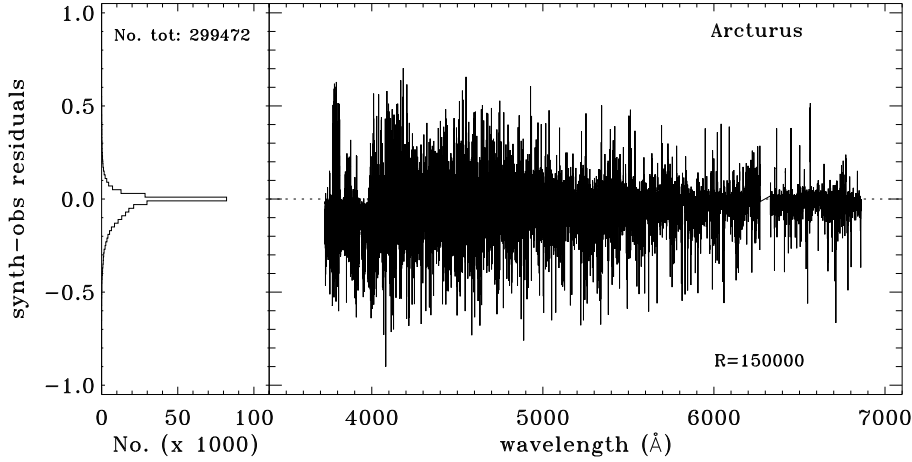[9] http://kurucz.harvard.edu/stars/ARCTURUS/modat4300g15kvd.dat

Fig. 5. Distribution of residual flux between the synthetic and observed spectrum of Arcturus. The observed SED is from Hinkle et al. (2000), at resolving power $R \sim 150\,000$. BLUERED synthetic spectrum assumes $(T_{\mathrm{eff}}/\log g/[M/H]) = (4300/1.5/-0.5)$ (with some elemental overabundance, see Table 2). According to the definitions of Fig. 2, the systematic offset between observed and synthetic spectra amounts to $\langle \Delta f_c/f_c \rangle = -0.037$, with a rms $\sigma(r)_{\mathrm{Arc}} = 0.108$ and a skewness $\gamma(r)_{\mathrm{Arc}} = -0.67$.

parameters of Arcturus are known with a much lower precision than the Sun; the values that we assumed are compatible with the recent estimation by Decin et al. (2003; $T_{\mathrm{eff}} = 4320 \pm 140$ K, $\log g = 1.5 \pm 0.15$; $[M/H] = -0.5 \pm 0.2$).

We obtained the synthetic spectrum with the same procedure used for the computation of the BLUERED grid, at a resolving power $R = 500\,000$. The normalized spectrum, which we obtained by dividing the emitted flux by the continuum value, has been broadened in the same way as the Sun to account for rotational and macroturbulence velocities of 1.5 km s^{-1} and 5.2 km s^{-1} (Gray & Brown 2006), respectively, and convolved with a Gaussian kernel to match the resolving power of the observation.

As for the Sun, Fig. 5 shows the corresponding residual flux distribution for Arcturus' SED, as well. In the comparison with the observations, we excluded the wavelength intervals 6270−6330 and 6860−7000 Å because of the presence of telluric bands. The systematics in residual distribution amounts to $\langle \Delta f_c/f_c \rangle = -0.037$, with a rms $\sigma(r)_{\mathrm{Arc}} = 0.108$, and a skewness of $\gamma(r)_{\mathrm{Arc}} = -0.67$. To compare consistently, if we broadened the solar spectrum to the Arcturus resolution and velocity dispersion, the solar rms would decrease to $\sigma(r)_\odot = 0.070$. On the other hand, if Arcturus' observed SED matched the Sun's wavelength range (including the missing 230 Å interval in the blue extreme), then $\sigma(r)_{\mathrm{Arc}}$ would probably have increased slightly.

The residual flux distribution of Arcturus' SED presents the same global characteristics as the solar one: it is strongly peaked at about the zero value and it presents a noticeable asymmetry, showing a wider (stronger) negative side, as the skewness value points out. The systematically lower synthetic flux at shortward of 4000 Å may partly originate from a discrepant determination of the continuum level: in fact, the lower temperature of Arcturus, which enhances the blanketing by metals, and a slightly lower spectral resolution of its observed spectrum, makes the normalization more difficult than in the solar case. Moreover, the physical parameters of Arcturus are less well determined with respect to the Sun: this higher uncertainty can also result in a higher rms. A higher comparison scatter, $\sigma(r)$, for Arcturus with respect to the Sun is in line with Bertone's et al. (2004a) previous findings, based on a low-resolution SED-fitting method to derive the main physical parameters of a sample of 334 stars along the full range of spectral types; actually, authors found a scatter $\sigma(r)$ of the best fit increased by about 30−50% moving from G2 to K1.5 stars.
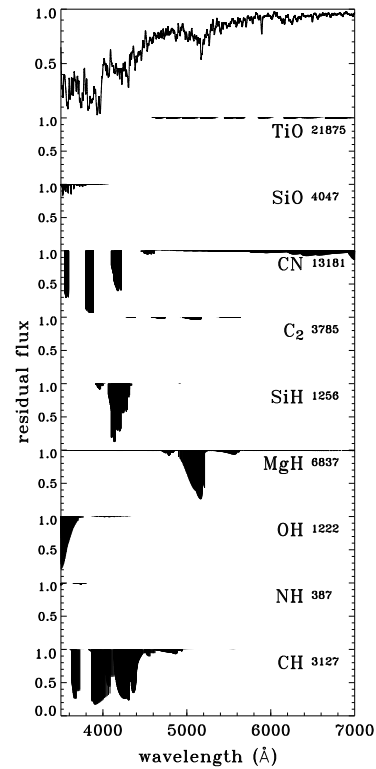

Fig. 6. The relative contribution to the integrated SED of Arcturus is singled out for different molecular species (each absorption line is represented by a vertical segment from the continuum level to the residual value of the central wavelength; the number of lines of each species is indicated on the panels). Note, among others, the strong MgH molecular bands in the optical spectral region, which affect the Mg$_1$, Mg$_2$, and Mg$_b$ spectroscopic indices. On the contrary, TiO absorption (with its largest number of absorbing lines) is almost negligible at the effective temperature and metallicity of Arcturus (abruptly increasing at the slightly cooler temperature of M stars). For a more immediate interpretation of the results, the spectrum of Arcturus (*top panel*) has been broadened to $R = 500$.

Due to the intrinsic non-monochromaticity of the absorption lines and the blending effect of the finite spectral resolution, in many cases observations alone cannot allow any univocal identification of every absorption feature evident in the spectrum. On the contrary, this is a straighforward task for the models, where we can selectively assess the contribution to the stellar SED of single chemical elements or molecules. With this aim, in Fig. 6
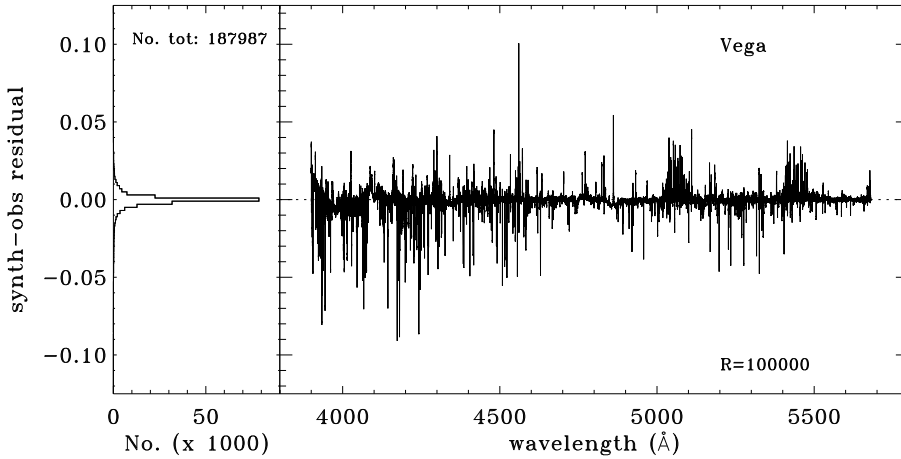
we carried out an illustrative experiment using the SYNTHE code to disaggregate the relative contribution of molecular blends and atomic lines to the integrated SED of Arcturus. Note, from the figure, that most of the strongest molecular bands (especially those of carbon-bearing molecules) are confined in the blue wavelength region of the spectrum, shortward of ∼4500 Å. As a "tricky" consequence of the prevailing contribution of the atomic blanketing in this spectral range, however, their apparent impact on the stellar SED can be easily masked. The only strong molecular absorption at redder wavelength is due to the MgH bands at about 5200 Å, which affects the Mg_1, Mg_2, and Mg_b Lick spectroscopic indices (e.g., Trager 1998). In spite of its largest total number of lines in the synthetic spectrum, one has to notice the nearly negligible absorption of TiO at the effective temperature and metallicity of Arcturus, this molecule becoming, on the contrary, a prevailing source of absorption in the SED of slightly cooler ($T_{\rm eff} \lesssim 3600$ K) M stars.

3.3. Vega and the high temperature regime

Thanks to its outstanding brightness, Vega (α Lyr, HD 172167, HR 7001; A0 V) is an ideal star to test the properties of the ATLAS-based synthetic spectra at the high $T_{\rm eff}$ regime. In spite of being one of the most studied stars and the major photometric standard, up to now few public spectra at high resolution exist (to our knowledge, Gulliver et al. 1991; Prugniel & Soubiran 2001; Bagnulo et al. 2003).

Takeda et al. (2007) have recently made public their spectrum of Vega, observed at $R \sim 100\,000$ and high S/N (∼1000−2000) over a large optical range (∼3900−8800 Å)[10]. The observations were carried out at the 1.88 m telescope at the Okayama Astrophysical Observatory with the High Dispersion Echelle Spectrograph (Izumiura 1999). They provide the normalized spectra of three different and partially overlapping intervals (3900−5100, 5000−6200, and 6000−7200 Å), which we merged to create a single spectrum over the 3900−7000 Å intervals.

To compute the synthetic spectrum of Vega we adopt the 81-layer ATLAS9 model atmosphere computed by Kurucz[11], which extends more toward the surface of the photosphere than the models used by Castelli & Kurucz (1994).

The main parameters are $T_{\rm eff} = 9550$ K; $\log g = 3.95$ dex; $[M/H] = -0.5$ dex (solar-scaled); and a constant microturbulence velocity of 2 km s^{-1}. These values are within the range defined by the results by several authors (Gulliver et al. 1994; Hill et al. 2004; Peterson et al. 2006). The synthetic spectrum, computed at $R = 500\,000$, was degraded to account for a projected rotational velocity of 21.9 km s^{-1} (Hill et al. 2004), and then it was broadened to $R = 100\,000$ to match the observed spectrum properties. We performed the comparison over a shorter wavelength interval (3900−5680 Å) than those we adopted for the Sun and Arcturus, because of the lack of observed data at the blue end and, at redder wavelengths, the pollution by telluric lines, which severely affects the distribution of the residuals. The difference between the synthetic and observed normalized flux is shown in Fig. 7, along with the projected histogram of the residual flux distribution.

The pseudo-continuum match in both the model and the observed spectrum is very good, leaving a negligible systematic offset $\langle\Delta f_{\rm c}/f_{\rm c}\rangle = -0.0008$; the residual scatter amounts to $\sigma(r)_{\rm Vega} = 0.007$, with a marked skewness $\gamma(r)_{\rm Vega} = -2.21$. As for the Sun and Arcturus, the skewness value indicates that the distribution presents a strong negative tail, which would have been even larger had we rejected the spurious contribution of some faint poorly corrected telluric lines about 5050 and 5450 Å, evident in the figure[12]. The results from the three reference stars indicate that the skewness increases with decreasing fit quality. This trend reflects the decreasing density of absorption lines: the residual distribution of Vega (left panel of Fig. 7) is dominated by the well-adjusted continuum, which makes the rms value smaller than for cooler stars, while the residuals corresponding to wavelength points where absorption lines are located show a clear asimmetry (right panel).

To properly compare these results with those of the Sun and Arcturus, we again applied our comparison procedure to the broadened spectra of the latter two stars to match the same resolution and rotation velocity of Vega. Over the wavelength interval 3900−5680 Å, the relevant values of the new rms estimates

---

[10] The data are available at http://pasj.asj.or.jp/v59/n1/590122/

[11] http://kurucz.harvard.edu/stars/VEGA/am05t9550g395k2.dat

[12] However, one has to consider that Vega is a pole-on fast rotating star (Gray 1988; Gulliver et al. 1994; Peterson et al. 2006; Aufdenberg et al. 2006); among other effects, this causes a flattened line profile, especially among faint lines, and leads to a systematic line-depth overestimate in the fitting synthetic SED. A more sophisticated modeling, in this regard, which should take into account the temperature variation over the stellar surface and the axis orientation, has been performed by Gulliver et al. (1994) and Aufdenberg et al. (2006) and is beyond the scope of the present analysis.

Table 3. Synthetic-observed rms with changing spectral resolution.

		Spectral resolution	
		$R = \lambda/\Delta\lambda$	
	522 000	150 000	100 000
Sun	0.089	0.070	0.045
Arcturus	...	0.108	0.088
Vega	...	...	0.007

The reported quantity is $\sigma(r)$, as defined in Footnote 5.

are summarized in the last Col. of Table 3. These new values of $\sigma(r)$ for Arcturus and the Sun are about a factor of two smaller than the corresponding scatter at higher resolution (see Col. 3 in the table), but are still nearly one order of magnitude higher than the Vega rms. We expected this result (Bertone et al. 2004a), considering the much lower line blanketing effect for Vega[13].

3.4. Comparison with the Prugniel & Soubiran library (R = 10 000)

To explore the behavior of the synthetic spectra of stars over the parameter space, we have carried out a comparison with the flux-calibrated spectra of Prugniel & Soubiran (2001). The spectra were obtained with the ELODIE echelle spectrograph at the Observatoire de Haute-Provence. They cover the wavelength range 4100–6800 Å at a resolving power of $R = 10\,000$, with a typical signal-to-noise ratio of 150 per pixel at 5550 Å, where the flux value was normalized. The broadband photometric precision is of the order of 2.5%. The total sample covers large intervals in spectral type, luminosity, and metallicity. These properties make this library suitable to extend the characterization of the synthetic grid to non-solar metallicities.

From the Prugniel & Soubiran (2001) database, we selected the 48 stars (excluding the Sun) with best flux calibration and most reliable physical parameters (reliability index of 4, according to authors' original classification, which means a ±80 K accuracy in the labeled $T_{\rm eff}$ and ±0.06 dex in $[M/H]$). For those stars with multiple observations, we coadded individual spectra to obtain one average SED. We excluded several small wavelength intervals (i.e., 5680–5695, 5859–5985, 6270–6325, 6510–6525, and 6735–6755 Å) from the analysis because of the presence of spectral glitches probably due to lags between echelle orders. The rejected intervals include, in particular, the region around the Na D doublet.

For each star, a synthetic SED with the corresponding combination of $T_{\rm eff}$, $\log g$, and $[M/H]$ was created by performing a trilinear interpolation within the BLUERED library domain. Since we avoided model extrapolation, three stars had to be excluded, falling outside the grid. We uniformed the synthetic spectra to the observations by normalizing the flux to unity at 5550 Å and broadening the spectra according to the procedure devised in Prugniel & Soubiran (2001). The convolution made use of a Gaussian kernel. The theoretical spectra were then resampled at the observed wavelength points. The final set of 45 stars accounted for in our analysis covers a $T_{\rm eff}$ interval between 4437 and 6589 K (i.e., spectral type between F and K), while surface gravity ranges between $\log g = 1.08$ and 4.6 dex, and metallicity spans the interval $[M/H] = -2.18$ to 0.15. A summary of the

[13] According to the ATLAS line database, in the wavelength interval considered for this comparison, the spectrum of Vega collects approximately 4800 absorption lines, while 31 200 lines are present in the Sun, and 55 600 in Arcturus).

Table 4. Physical parameters and BLUERED best-fit rms for the ELODIE stellar sample.

HD No.	Sp. type	$T_{\rm eff}$	$\log g$	$[M/H]$	rms
400	F8IV	6163	4.12	−0.29	0.040
1835	G3V	5771	4.44	0.15	0.079
3567	F5V	6000	4.03	−1.29	0.035
6582	G5Vp	5320	4.49	−0.76	0.052
10 700	G8V	5301	4.34	−0.50	0.072
25 329	K1V...	4801	4.60	−1.72	0.067
26 297	G5/G6IVw	4437	1.08	−1.69	0.084
34 411	G0V	5849	4.17	0.05	0.054
39 587	G0V	5913	4.40	−0.01	0.053
61 421	F5IV–V	6589	4.03	−0.01	0.033
64 606	G8V	5164	3.73	−0.95	0.059
76 932	F7/F8IV/V	5850	3.62	−0.92	0.081
87 141	F5V	6365	4.03	0.08	0.045
94 028	F4V	5952	4.22	−1.45	0.040
102 870	F8V	6108	4.18	0.15	0.049
104 979	G8III	4896	2.68	−0.33	0.089
109 358	G0V	5890	4.41	−0.11	0.057
113 226	G8IIIvar	4991	2.78	0.07	0.098
114 710	G0V	5979	4.40	0.08	0.055
114 762	F9V	5841	4.16	−0.72	0.049
115 383	G0Vs	5993	3.41	0.08	0.048
122 956	G6IV/Vw..	4634	1.45	−1.76	0.068
124 850	F7V	6141	3.97	−0.13	0.070
141 004	G0Vvar	5912	3.53	−0.01	0.056
150 177	F3V	6136	3.99	−0.56	0.060
157 089	F9V	5784	4.14	−0.55	0.052
173 667	F6V	6338	4.09	−0.11	0.048
174 912	F8	5873	4.37	−0.45	0.046
175 305	G5III	5073	2.51	−1.44	0.050
186 408	G2V	5820	4.26	0.07	0.058
186 427	G5V	5762	4.38	0.06	0.063
187 691	F8V	6101	4.22	0.09	0.052
189 558	G0/G1V	5637	3.24	−1.13	0.047
194 598	F7V–VI	5961	4.30	−1.16	0.047
197 989	K0III	4766	2.56	−0.10	0.106
201 891	F8V–VI	5895	4.41	−1.05	0.056
204 543	G0	4683	1.30	−1.79	0.093
207 978	F6IVwvar	6275	4.03	−0.57	0.054
208 906	F8V–VI	5966	4.21	−0.72	0.052
215 648	F7V	6155	4.11	−0.30	0.043
216 143	G5	4506	1.21	−2.18	0.095
216 385	F7IV	6200	3.98	−0.32	0.043
217 014	G5V	5757	4.23	0.15	0.066
222 368	F7V	6154	3.69	−0.22	0.036
224 930	G2V	5324	4.47	−0.75	0.075

sample characteristic is reported in Table 4, while the location of stars in the $\log g - T_{\rm eff}$ diagram is displayed in Fig. 8.

Since we are dealing with absolute flux-calibrated spectra, we adopted, as a goodness of fit indicator, the rms of the relative flux residuals $r'' = [(f_{\rm syn}/f_{\rm obs}) - 1]$. Due to the different physical variables and different spectral resolutions and ranges, the rms absolute values of the ELODIE sample cannot be directly compared with those of the Sun, Arcturus, and Vega. In Fig. 9, we show an example of the comparison between observed and theoretical SEDs for the F-type star HD 61421, one of the best rms cases. Even for this star, however, with a closer analysis we notice a clear oscillatory trend of flux residuals, evidently reminiscent of flux-calibration uncertainties.

As for the case of Arcturus and the Sun, the more extended comparison with the whole ELODIE sample also confirms the increasingly poor match performances of synthetic models when fitting the observed SEDs at shorter wavelengths. For F-type
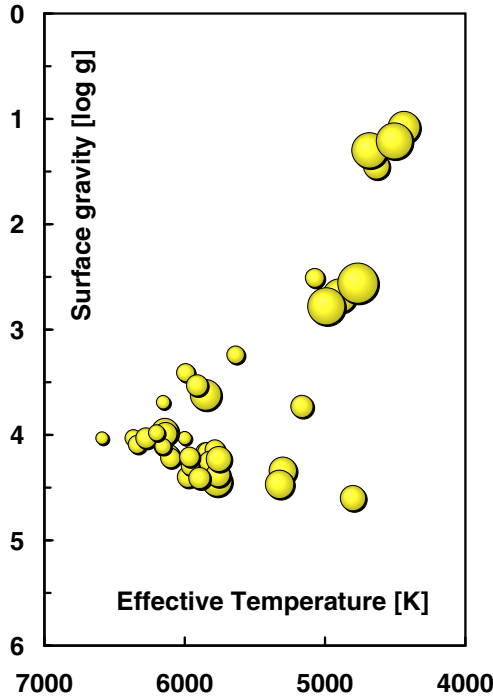
Fig. 8. The location of the 45 reference stars from the ELODIE spectral sample in the $(\log g - T_{\text{eff}})$ plane. Dot size is proportional to the BLUERED best-fit rms according to Table 4, with bigger dots implying a poorer fit.
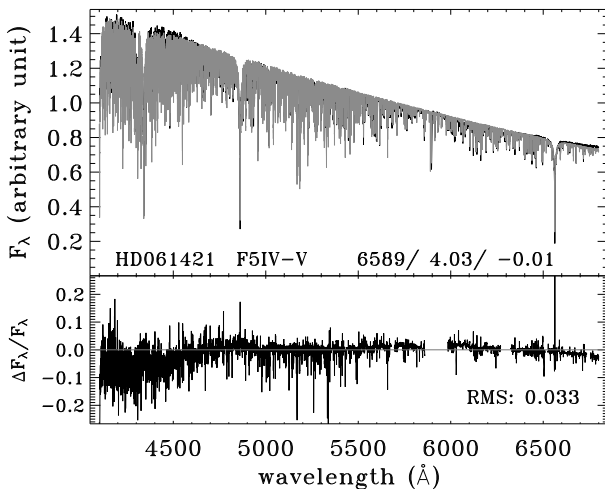

Fig. 9. ELODIE spectrum of HD 61421. In the upper panel, the SYNTHE spectrum (*grey line*) is superimposed on the observed spectrum (*black line*). The relative flux residual is plotted in *the lower panel*.

stars, such as the one in Fig. 9, the core of Balmer lines is not well reproduced, causing large positive spikes in the residuals. The mismatch is due to a poorer LTE approximation for the very upper atmosphere layers, which contribute to the line-core photons; definitely, a much better fit could be achieved adopting a NLTE treatment for these outermost atmosphere regions (Przybilla & Butler 2004).

We report the BLUERED best-fit rms (Col. 6 of Table 4), as a function of the stellar physical parameters, in Fig. 10. For a more general view of the sample, the same value is also proportional to dot size in the plot of Fig. 8. A correlation with the effective temperature and surface gravity seems quite evident: the match

improves by a factor of two when moving from K to F stars, and from supergiants to dwarfs. While the trend with the T_{eff} reflects the number of absorption lines present in the spectra, the poorer fit of low-gravity stars may also be caused by the plane-parallel approximation of BLUERED input model atmospheres. On the contrary, no evident trend of residuals is present vs. stellar metallicity (forcedly restraining, however, to the prevailing (sub)-solar metal abundance of the observed sample).

4. Summary and conclusions

In this work we carried out a detailed analysis of the Kurucz (1993a) theoretical "corpus" of stellar atmosphere models, relying on the original ATLAS/SYNTHE synthesis codes. This makes part of a more general "validation" process undertaken by, e.g., Bessell et al. (1998), Castelli et al. (1997), and Martins & Coelho (2007). The motivation for a supplementary effort to more firmly assess the real capabilities of the theoretical framework comes from the extremely wide range of applications of the Kurucz models. These models are often a central reference tool for the astrophysical investigation of single stars, as well as stellar systems (through population synthesis procedures). In this regard, it is clear that any claimed predictive power of the models is strictly constrained by the limits (in accuracy and completeness) of the implemented input physics to properly trace the atmospheric structure and thereby produce a realistic picture of the synthetic SED for stars along the entire range of temperature and chemical composition.

Facing this formidable task, the revised set of the atmosphere models that stemmed from the ATLAS9 code and its later followup successfully tackled a number of important problems, dealing, for instance, with metal blanketing, molecular contribution to the atmosphere opacity in cool stars, or to the striking deviations from the LTE conditions that occur, under special circumstances, in upper atmospheric layers of hot stars. Although improved, all these issues still leave ample space for further refinements and fine tuning of the theory, especially necessary due to the intervening wealth of spectroscopic observations from new-generation telescopes at unprecedented high resolution.

Relying on the Kurucz SYNTHE code, we therefore decided to carry the computation of synthetic stellar SED to its most extreme limit, covering the whole ATLAS9 grid of model atmospheres at $R = 500\,000$. This theoretical library of 832 synthetic spectra, which we named BLUERED (see Sect. 2 and Table 1), provides the ultimate reference tool for any in-depth browsing of the "fine structure" hidden in the overall SED of stars. The comparison with three outstanding reference templates, namely the Sun and the two very bright stars, Arcturus and Vega, has been the natural "acid test" to probe three central topics in the physical framework, still open to debate.

In particular, the match of the Kurucz et al. (1984) solar atlas (see Sect. 3.1) neatly confirms the apparent "excess" of theoretical line blanketing. We have shown in Fig. 2 that, at the assumed spectral resolution, the mismatch induces a relative scatter in the continuum-normalized flux of the order of $\simeq 9\%$, a value that significantly exceeds the induced uncertainty of systematics in the pseudo-continuum setting (contributing a scarce 1.5%).

The mismatch with such a preeminent target might evidently reverberate in a much wider context, for instance when using the SED fitting method to derive chemical abundances or other fundamental parameters of stars. In fact, more strong-lined synthetic spectra would require, for instance, slightly higher fitting temperature or slightly lower metal abundance to match the observed spectral pattern in a given (continuum-normalized) SED.
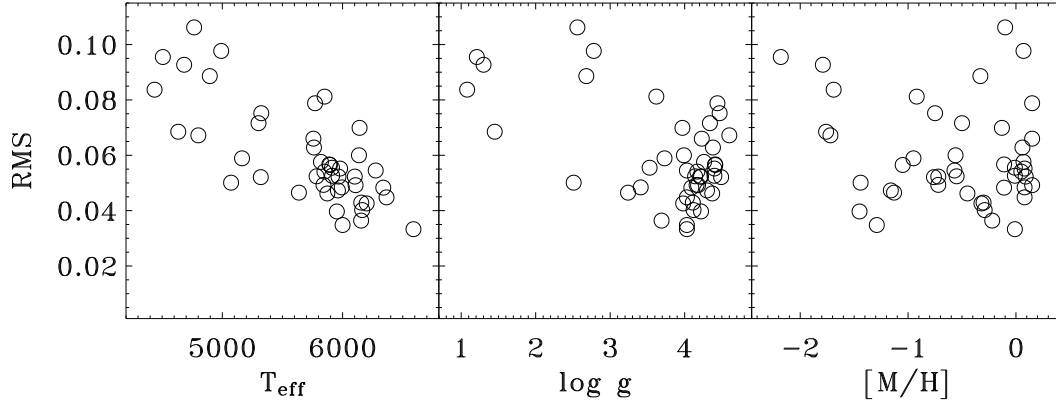
Fig. 10. rms of the comparison between synthetic and Elodie spectra versus the three leading stellar parameters (effective temperature, surface gravity and metallicity). Note, in particular, the improved fit with increasing T_{eff} and $\log g$.

This case has been directly verified with the Sun, for which the unconstrained best fit of the normalized spectrum demands a metallicity of half the "solar" value and a 83 K warmer effective temperature; the latter value further raises to $\Delta T_{eff} = +353$ K, if we force the fit with a nominal "solar" metal abundance.

Clearly, the effect points to an important (and yet unavoidable) revision process of the atomic transitions database requiring, among other things, the appropriate fine tuning of the oscillator-force $[\log(gf)]$ parameters. The results on an exploratory experiment (Fig. 4) actually demonstrate that a systematic decrease of $\log(gf)$ by ~40%, especially for the iron atomic transitions, helps alleviate the discrepancy with the observations. However, only an "ad hoc" refinement of the transition parameters of *each individual* spectral feature could really lead to a firm improvement of the situation.

Spectral synthesis at the K-giant temperature regime has been explored through the case of Arcturus (Sect. 3.2). For this star, $R = 150\,000$ optical observations by Hinkle et al. (2000) have been matched by tuning metal abundance to account for a non-solar chemical partition. The relevant aspect of the Arcturus fit deals with the Atlas real capability of handling the overall contribution of molecular bands, which begin to emerge at about 4000 K and become by far the prevailing source of continuum absorption for late (M and later) spectral types. To improve our analysis, for our calculations we updated the Kurucz' original list of TiO transitions by including the expanded compilation by Schwenke (1998). While reassuring as to the continuum fit (systematic offset, along the wavelength range of the observations, i.e., $\lambda\lambda\,3727-7000$ Å is less than a ~4%), the intrinsic scatter of the relative flux residuals is far higher than the Sun, considering that the lower spectral resolution, by itself, acts in the sense of "smoothing" the SED, thus reducing the $\Delta f/f$ rms (see Table 3).

Three important features of theoretical fitting of cool stars are worth of attention: *i)* most molecular absorption occurs in the blue, shortward of 4500 Å. This is especially the case of the compounds that contain carbon (CH, CN) and silicon (SiO, SiH), which could heavily modulate the location of pseudo-continuum and might, therefore, indirectly affect the strength of narrow-band spectrophotometric indices in this spectral range; *ii)* at longer wavelength, Magnesium hydride (MgH) is the strongest feature, extensively blending the corresponding atomic transitions about 5200 Å, which are accounted for, for instance, in the popular Mg_2 Lick index; *iii)* Titanium oxide and CN band systems are pervasive longward of ~5000 Å, but their strength vanishes at the temperature regime of K stars ($T_{eff} \gtrsim 4000$ K),

and abruptly increases among M (and later) stars. As for MgH, a proper accounting of the TiO effects might be of crucial importance for a correct intepretation of narrow-band indices (again, like Mg_2) at optical wavelengths (see, e.g., Tantalo & Chiosi 2004, for a special emphasis on this issue).

These figures, together with the direct rms estimates of Table 3, make a somewhat quantitative point of the main recognized difficulty of Kurucz' models, namely the increasingly poor accounting of late-type stars when moving cooler than ~4000 K. Actually, we can place a still unsurmounted limit at $T_{eff} \lesssim 3000$ K where, in addition to diatomic molecule contribution, one should also account for the intervening effect of tri-atomic particles (especially water vapor, H_2O). Among others, this limitation poses serious constraints to population synthesis models (especially at high metallicity), as a substantial part of red-giant evolution cannot be properly reproduced, in terms of colors and/or integrated SED, from the theoretical point of view alone. This is briefly sketched in Fig. 11 for the illustrative case of an old simple stellar population of solar metallicity. There are hints that such a problem with late-type stellar fit might unfortunately be more endemic and pervasive than supposed (Bertone et al. 2004a), as confirmed for instance by the match with even more sophisticated computational schemes, like Hauschildt's et al. (1999) NextGen models[14].

A final case of "primary" template stars in our analysis concerns Vega, as a special "probe" of Kurucz' model performance at the high-temperature regime (Sect. 3.3). To this aim, in Fig. 7 we fitted the continuum-normalized spectrum by Takeda et al. (2007), taken at $R = 100\,000$ along the wavelength range $\lambda\lambda\,3900-5680$ Å. The results of this comparison confirm the overall trend of our experiments, validating the increasing accuracy of Kurucz' theoretical framework with increasing effective temperature. By comparing homogenously with the case of Arcturus and the Sun, we find that Vega is reproduced within a roughly one order of magnitude better accuracy (see the fourth Col. of Table 3). On the one hand, this is a somewhat natural consequence of less severe blanketing effects (compared with Arcturus and the Sun over a common wavelength window, Vega SED displays roughly one order of magnitude fewer absorption features). On the other hand, a marked skewness in the fitting flux residuals has to be reported $[\gamma(r)_{Vega} = -2.21]$, indicating

---

[14] Among others, NextGen models assume a spherical geometry for the atmosphere layers of low-gravity stars and important improvements in the direct and self-consistent calculation of monochromatic chemical opacity.
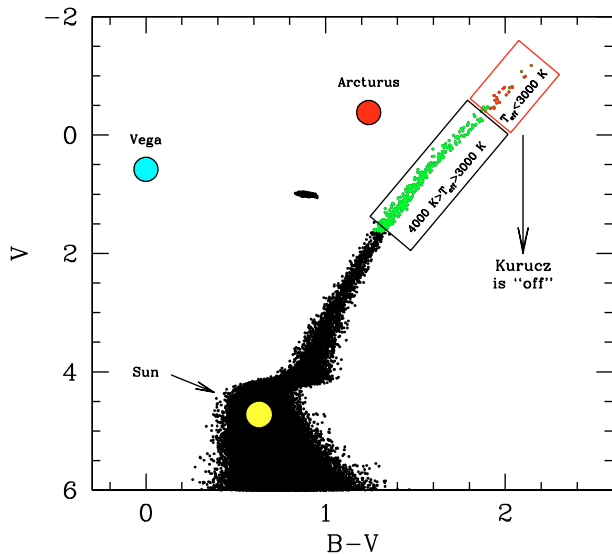
Fig. 11. The illustrative c-m diagram of a 15 Gyr theoretical simple stellar population of solar metallicity, from Buzzoni (1989). The effective temperature range along red-giant evolution is marked on the plot. Molecular contribution starts becoming increasingly relevant for K-stars cooler than ~4000 K, while for $T_{eff} \lesssim 3000$ K Kurucz models cannot safely reproduce stellar SED due to the appearance of pervasive absorption bands of tri-atomic molecules in stellar SED. The location of the three reference templates in our discussion, namely the Sun, Arcturus and Vega is overplotted for clarity.

the systematic presence of too "spiked" theoretical features compared with the observed SED.

This effect is partly the consequence of the increasing inadequacy of the LTE approximation with increasing temperature (non-LTE models, in general predict a shallower blanketing as a result of a weaker core of faint lines, see the discussion in Rodriguez-Merino et al. 2005); however, for the specific case of Vega, such enhanced skewness in the SED best fit might also account for the pole-on fast rotating geometry of the star, which causes the line profile to flatten (Aufdenberg et al. 2004). Quite interestingly, and as a general suggestion, one could even take advantage of the skewness test as a simple and very immediate diagnostic tool to probe "hidden" stellar rotation.

The main conclusions from the analysis of our three main reference stars are confirmed, on a more general basis, when compared with the larger dataset of stars in the ELODIE spectral library (45 stars, observed at $R = 10\,000$, cf. Table 4). In the latter case, however, error sources are more composite (contrary to the normalized spectra of the Sun, Arcturus, and Vega, for the ELODIE stars we performed a BLUERED best fit of the absolute flux-calibrated SED, see, e.g., Fig. 9) and cannot, therefore, be compared in a straightforward manner with rms estimates of Table 3.

Nevertheless, the rms distribution vs. fundamental stellar parameters, according to Fig. 10, confirms that ATLAS synthetic spectra are better suited to fitting warm stars, providing over a factor of two better fit for F stars compared to G/K stars. As for the temperature, a nice trend is also detected vs. surface gravity (dwarfs are better fitted than giants), but one should be aware of a possible selection effect as the sample lacks warm supergiants (see Fig. 8), and of the limitations of plane-parallel model atmospheres. Interestingly enough, Fig. 10 shows that no apparent residual drift is present with metallicity, a feature that confirms the prevailing role of overall thermodynamical conditions

(especially the temperature structure along the atmospheric layers) in constraining line strength for a given chemical element rather than its absolute abundance.

References

Alonso, A., Arribas, S., & Martínez-Roger, C. 1999, A&AS, 140, 261
Anders, E., & Grevesse, N. 1989, Geochim. Cosmochim. Acta, 53, 197
Aufdenberg, J. P., Ludwig, H.-G., & Kervella, P. 2004, AAS Bull., 205, 1203
Aufdenberg, J. P., Mérand, A., Coudé du Foresto, V., et al. 2006, ApJ, 645, 664
Barbuy, B., Perrin, M.-N., Katz, D., et al. 2003, A&A, 404, 661
Bagnulo, S., Jehin, E., Ledoux, C., et al. 2003, The Messenger, 114, 10
Behara, N. T., & Jeffery, C. S. 2006, A&A, 451, 643
Bell, R. A., Paltoglou, G., & Tripicco, M. J. 1994, MNRAS, 268, 771
Bertone, E. 2001, Ph.D. Thesis, Università di Milano
Bertone, E., Buzzoni, A., Rodríguez-Merino, L. H., & Chávez, M. 2003a, in Proc. of Modelling of Stellar Atmospheres, ed. N. Piskunov, W. W. Weiss, & D. F. Gray (San Francisco: ASP), IAU Symp., 210, A1
Bertone, E., Buzzoni, A., Chávez, M., & Rodríguez-Merino, L. H. 2003b, in Proc. of the MPA workshop on Stellar Populations 2003, available in electronic form at http://www.mpa-garching.mpg.de/stelpops
Bertone, E., Buzzoni, A., Chávez, M., & Rodríguez-Merino, L. H. 2004a, AJ, 128, 829
Bertone, E., Buzzoni, A., Rodríguez-Merino, L. H., & Chávez, M. 2004b, Mem. SAIt, 75, 158
Bertone, E., Chavez, M., Rodriguez-Merino, L. H., & Buzzoni, A. 2005, in Proc. of Resolved Stellar Populations, ed. M. Chavez, & D. Valls-Gabaud (San Francisco: ASP), ASP Conf. Ser., in press
Bessell, M. S., Castelli, F., & Plez, B. 1998, A&A, 333, 231
Brekke, P. 1993, ApJS, 87, 443
Bruzual, G., & Charlot, S. 2003, MNRAS, 344, 1000
Böhm-Vitense, E. 1958, Z. Astrophys., 46, 108
Böhm-Vitense, E. 1981, ARA&A, 19, 295
Buzzoni, A. 1989, ApJS, 71, 817
Buzzoni, A. 2005, MNRAS, 361, 725
Buzzoni, A., Chavez, M., Malagnini, M. L., & Morossi, C. 2001, PASP, 113, 1365
Buzzoni, A., Bertone, E., Rodriguez-Merino, L. H., & Chavez, M. 2005, in Proc. of Multiwavelength Mapping of Galaxy Formation and Evolution, ed. A. Renzini, & R. Bender, ESO Conf. Ser. (Springer: Heidelberg), 361
Castelli, F., & Kurucz, R. L. 1994, A&A, 281, 817
Castelli, F., & Kurucz, R. L. 2001, A&A, 372, 260
Castelli, F., & Munari, U. 2001, A&A, 366, 1003
Castelli, F., Gratton, R. G., & Kurucz, R. L. 1997, A&A, 318, 841
Cayrel, R., Perrin, M.-N., Barbuy, B., & Buser, R. 1991, A&A, 247, 108
Chavez, M., Malagnini, M. L., & Morossi, C. 1997, A&AS, 126, 267
Cohen, L. 1981, An atlas of solar spectra between 1175 and 1950 Å recorded on SKYLAB with the NRL's Apollo telescope mount experiment, NASA Ref. Pub., 1069
Coelho, P., Barbuy, B., Meléndez, J., Schiavon, R. P., & Castilho, B. V. 2005, A&A, 443, 735
Decin, L., Vandenbussche, B., Waelkens, C., et al. 2003, A&A, 400, 709
Delbouille, L., Roland, G., & Neven, L. 1973, Atlas photometrique du spectre solaire de λ3000 a λ10000 (Liège: Université de Liège, Inst. d'Astrophysique)
di Benedetto, G. P. 1998, A&A, 339, 858
di Benedetto, G. P., & Rabbia, Y. 1987, A&A, 188, 114
Faber, S. M., Friel, E. D., Burstein, D., & Gaskell, C. M. 1985, ApJS, 57, 711
Girardi, L., Bressan, A., Bertelli, G., & Chiosi, C. 2000, A&AS, 141, 371
Gonzalez Delgado, R. M., & Leitherer, C. 1999, ApJS, 125, 479
Gray, D. F., & Brown, K. I. T. 2006, PASP, 118, 1112
Gray, R. O. 1988, JRASC, 82, 336
Griffin, R. F. 1968, A Photometric Atlas of the Spectrum of Arcturus λλ 3600−8825 Å (Cambridge: Cambridge Philos. Soc.)
Gulliver, A. F., Adelman, S. J., Cowley, C. R., & Fletcher, J. M. 1991, ApJ, 380, 223
Gulliver, A. F., Hill, G., & Adelman, S. J. 1994, ApJ, 429, L81
Gunn, J. E., & Knapp, G. R. 1993, in proc. of Sky Surveys: Protostars to Protogalaxies, ed. B. T. Soifer (ASP: San Francisco), ASP Conf. Ser., 43, 267
Gurtovenko, E. A., & Kostik, R. I. 1981, A&AS, 46, 239
Gustafsson, B., Bell, R. A., Eriksson, K., & Nordlund, Å 1975, A&A, 42, 407

Hall, D. N. B. 1973, An atlas of infrared spectra of the solar photosphere and of sunspot umbrae, in the spectral intervals 4040 cm^{-1}−5095 cm^{-1}; 5550 cm^{-1}−6700 cm^{-1}; 7400 cm^{-1}−8790 cm^{-1} (Tucson: Kitt Peak Nat. Obs.)

Hauschildt, P. H., Allard, F., & Baron, E. 1999a, ApJ, 512, 377

Hauschildt, P. H., Allard, F., Ferguson, J., Baron, E., & Alexander, D. R. 1999b, ApJ, 525, 871

Hill, G., Gulliver, A. F., & Adelman, S. J. 2004, in Proc. of The A-Star Puzzle, ed. J. Zverko, J. Ziznovsky, S. J. Adelman, & W. W. Weiss, IAU Symp., 224, 35

Hillier, D. J., & Miller, D. L. 1998, ApJ, 496, 407

Hinkle, K., Wallace, L., Valenti, J., & Harmer, D. 2000, Visible and Near Infrared Atlas of the Arcturus Spectrum 3727−9300 Å (San Francisco: ASP)

Hinkle, K., Wallace, L., Valenti, J., & Ayres, T. 2005, Ultraviolet Atlas of the Arcturus Spectrum 1150−3800 Å (San Francisco: ASP)

Hubeny, I., & Lanz, T. 1992, A&A, 262, 501

Hubeny, I., & Lanz, T. 1995, ApJ, 439, 875

Izumiura, H. 1999, in Proc. 4th East Asian Meeting on Astronomy, Observational Astrophysics in Asia and its Future, ed. P. S. Chen (Kunming: Yunnan Observatory), 77

Johnson, H. L. 1966, ARA&A, 4, 193

Katz, D., Munari, U., Cropper, M., et al. 2004, MNRAS, 354, 1223

Kurucz, R. L. 1970, SAO Special Report, 309

Kurucz, R. L. 1979, ApJS, 40, 1

Kurucz, R. L. 1992a, Proc. IAU Symp. 149, ed. B. Barbuy, & A. Renzini (Dordrecht: Kluwer), 225

Kurucz, R. L. 1992b, RMxAA, 23, 45

Kurucz, R. L. 1993a, CD-ROM 13, ATLAS9 Stellar Atmosphere Programs and 2 km s^{-1} Grid (Cambridge, Smithsonian Astrophys. Obs.)

Kurucz, R. L. 1993b, CD-ROMs 1, 15 and 18, SYNTHE Spectrum Synthesis Programs and Line Data (Cambridge: Smithsonian Astrophys. Obs.)

Kurucz, R. L. 1995, Proc. of Laboratory and Astronomical High Resolution Spectra, ed. A. J. Sauval, R. Blomme, & N. Grevesse (San Francisco: ASP), ASP Conf. Ser., 81, 583

Kurucz, R. L. 1999, CD-ROM No. 24, The TiO revised line list

Kurucz, R. L., Furenlid, I., Brault, L., & Testerman, L. 1984, Solar flux atlas from 296 to 1300 nm, National Solar Observatory Atlas, Sunspot, New Mexico, Nat. Sol. Obs.

Leonardi, A. J., & Rose, J. 2003, AJ, 126, 1811

Luck, R. E., & Heiter, U. 2005, AJ, 129, 1063

Martins, L. P., & Coelho, P. 2007, MNRAS, 381, 1329

Martins, L. P., González Delgado, R. M., Leitherer, C., Cerviño, M., & Hauschildt, P. 2005, MNRAS, 358, 49

McAllister, H. C. 1960, A preliminary photometric atlas of the solar ultraviolet spectrum from 1800 to 2965 Å (Boulder: Univ. of Colorado)

Milone, A., & Barbuy, B. 1994, A&AS, 108, 449

Milone, E. F., Palm Schneider, W., Tilford, S. G., & Tousey, R. 1974, An atlas of the solar ultraviolet spectrum between 2220 and 2990 Å, BAAS, 6, 292

Minnaert, M., Houtgast, J., & Mulders, G. F. W. 1940, Photometric atlas of the solar spectrum from λ 3612 to λ 8771 with an appendix from λ 3332 to λ 3637 (Utrecht: Sterrewacht Sonnenborgh)

Mohler, O. 1950, Photometric atlas of the near infra-red solar spectrum, λ 8465 to λ 25 242 (Ann Arbor: University of Michigan Press)

Munari, U., & Castelli, F. 2000, A&AS, 141, 141

Munari, U., Sordo, R., Castelli, F., & Zwitter, T. 2005, A&A, 442, 1127

Murphy, T., & Meiksin, A. 2004, MNRAS, 351, 1430

Pauldrach, A. W. A., Hoffmann, T. L., & Lennon, M. 2001, A&A, 375, 161

Peterson, R. C., Dorman, B., & Rood, R. T. 2001, ApJ, 559, 372

Peterson, D. M., Hummel, C. A., Pauls, T. A., et al. 2006, Nature, 440, 896

Pierce, A. K., & Lopresto, J. C. 1984, SoPh, 93, 155

Prugniel, Ph., & Soubiran, C. 2001, A&A, 369, 1048

Przybilla, N., & Butler, K. 2004, ApJ, 610, L61

Ridgway, S. T., Joyce, R. R., White, N. M., & Wing, R. F. 1980, ApJ, 235, 126

Rodriguez-Merino, L. H., Chavez, M., Bertone, E., & Buzzoni, A. 2005, ApJ, 626, 411

Rose, J. A. 1994, AJ, 107, 206

Ryde, N., Lambert, D. L., Richter, M. J., & Lacy, J. H. 2002, ApJ, 580, 447

Rutten, R. J. 1988, Physics of Formation of FE II Lines Outside LTE, IAU Colloq., 94, 185

Salasnich, B., Girardi, L., Weiss, A., & Chiosi, C. 2000, A&A, 361, 1023

Samain, D. 1995, A&AS, 113, 237

Santolaya-Rey, A. E., Puls, J., & Herrero, A. 1997, A&A, 323, 488

Schwenke, D. W. 1998, Faraday Discuss, 109, 321

Shchukina, N., & Trujillo Bueno, J. 2001, ApJ, 550, 970

Short, C. I., & Hauschildt, P. H. 2003, ApJ, 596, 501

Short, C. I., & Hauschildt, P. H. 2005, ApJ, 618, 926

Shulyak, D., Tsymbal, V., Ryabchikova, T., Stütz, C., & Weiss, W. W. 2004, A&A, 428, 993

Soubiran, C., Katz, D., & Cayrel, R. 1998, A&AS, 133, 221

Spite, M. 1967, Ann. d'Astroph., 30, 211

Steinmetz, M. 2003, in ASP Conf. Ser., ed. U. Munari (San Francisco: ASP), 298, 381

Strom, S. E., & Kurucz, R. L. 1966, JQSRT, 6, 591

Takeda, Y., Kawanomoto, S., & Ohishi, N. 2007, PASJ, 59, 245

Tantalo, R., & Chiosi, C. 2004, MNRAS, 353, 917

Thuillier, G., Herse, M., Simon, P. C., et al. 1997, SoPh, 171, 283

Trager, S. C., Worthey, G., Faber, S. M., Burstein, D., Gonzalez, J. J. 1998, ApJS, 116, 1

Tsuji, T. 1976, PASJ, 28, 543

Valenti, J. A., & Fischer, D. A. 2005, ApJS, 159, 141

Vazdekis, A., & Arimoto, N. 1999, ApJ, 525, 144

Vazdekis, A., Casuso, E., Peletier, R. F., & Beckman, J. E. 1996, ApJS, 106, 307

Wallace, L., & Hinkle, K. 1996, ApJS, 103, 235

Wallace, L., Livingston, W., Hinkle, K., & Bernath, P. 1996, ApJS, 106, 165

Werner, K. 1986, A&A, 161, 177

Wittkowski, M., Aufdenberg, J. P., & Kervella, P. 2004, A&A, 413, 711

Worthey, G. 1994, ApJS, 95, 107

Worthey, G., Faber, S. M., Gonzalez, J. J., & Burstein, D. 1994, ApJS, 94, 687

Yi, S., Demarque P., & Oemler, A. J. 1998, ApJ, 492, 480